A Multisensory Zone in Rat Parietotemporal Cortex: Intra- and Extracellular Physiology and Thalamocortical Connections

BARBARA BRETT-GREEN,[1] EVA FIFKOVÁ,[1] DAVID T. LARUE,[2]
JEFFERY A. WINER,[2] AND DANIEL S. BARTH[1]*
[1]Department of Psychology, University of Colorado at Boulder, Boulder, Colorado 80309
[2]Department of Molecular and Cell Biology, University of California at
Berkeley, Berkeley, California 94720

ABSTRACT

Multisensory integration is essential for the expression of complex behaviors in humans and animals. However, few studies have investigated the neural sites where multisensory integration may occur. Therefore, we used electrophysiology and retrograde labeling to study a region of the rat parietotemporal cortex that responds uniquely to auditory and somatosensory multisensory stimulation. This multisensory responsiveness suggests a functional organization resembling multisensory association cortex in cats and primates. Extracellular multielectrode surface mapping defined a region between auditory and somatosensory cortex where responses to combined auditory/somatosensory stimulation were larger in amplitude and earlier in latency than responses to either stimulus alone. Moreover, multisensory responses were nonlinear and differed from the summed unimodal responses. Intracellular recording found almost exclusively multisensory cells that responded to both unisensory and multisensory stimulation with excitatory postsynaptic potentials (EPSPs) and/or action potentials, conclusively defining a multisensory zone (MZ). In addition, intracellular responses were similar to extracellular recordings, with larger and earlier EPSPs evoked by multisensory stimulation, and interactions suggesting nonlinear postsynaptic summation to combined stimuli. Thalamic input to MZ from unimodal auditory and somatosensory thalamic relay nuclei and from multisensory thalamic regions support the idea that parallel thalamocortical projections may drive multisensory functions as strongly as corticocortical projections. Whereas the MZ integrates uni- and multisensory thalamocortical afferent streams, it may ultimately influence brainstem multisensory structures such as the superior colliculus. J. Comp. Neurol. 460:223–237, 2003.   © 2003 Wiley-Liss, Inc.

Indexing terms: mapping; evoked potentials; multimodal; polysensory

A basic task of the central nervous system is to integrate information from the separate senses, enabling an animal to behave adaptively in a demanding environment. For integration to occur, anatomic convergence of the separate sensory pathways is required. Sites for multisensory convergence include the superior colliculus (Stein and Meredith, 1993), the thalamus (Steriade et al., 1997), and the cortex. In fact, studies in primates (Jones and Powell, 1970; Benevento et al., 1977; Bruce et al., 1981; Pandya and Yeterian, 1985; Hikosaka et al., 1988; Schroeder et al., 2001) and cats (Berman, 1961; Fishman and Micheal, 1973; Schneider and Davis, 1974; Clemo and Stein, 1983; Roda and Reinoso-Suárez, 1983; Toldi and Fehér, 1984; Toldi et al., 1984; Wallace et al., 1992) find multisensory convergence in several upstream cortical association areas

that may be essential for executive levels of sensory function (Pandya and Yeterian, 1985). These association areas

may integrate input across modalities, enabling the perceptual processing that must precede motor planning (Mesulam, 1998). Such areas, which may be expanded in higher mammals, may be part of a network for spatial reference that enables goal directed movements (Hyvärinen, 1982).

A smaller set of studies have also identified putative multisensory zones in the rat cortex (Toldi et al., 1984, 1986; Di et al., 1994; Jiang et al., 1994; Barth et al., 1995), suggesting that it may have functional subdivisions comparable to those in cats and primates. To explore this issue, we have mapped uni- and multisensory responses at high spatial resolution with multielectrode arrays placed on the cortical surface. We find that both click-elicited auditory evoked potentials (AEPs) and somatosensory evoked potentials (SEPs) elicited by vibrissal stimulation, have their largest amplitude and earliest poststimulus latency within primary auditory (AI) cortex and the vibrissal representation of primary somatosensory cortex, the barrel field (SIbf; Barth and Di, 1990, 1991; Di and Barth, 1991). However, both the AEP and SEP extend well beyond these borders, with longer latency responses evident in the fields outside AI and SI. These fields are collectively designated as nonprimary and are classified as the secondary auditory (AII) and secondary somatosensory (SII) cortex, respectively. Although the spatiotemporal distributions of the short latency AEP and SEP are largely segregated, the longer latency responses occupy a common cortical space between AI and SIbf (Di et al., 1994). Moreover, responses evoked here by joint auditory and somatosensory stimulation (ASEP) differ from the simple linear sum of the separate AEP and SEP, indicating a unique and localized process that cannot be the result of linear superposition of volume-conducted currents from adjacent unisensory cortices, and suggesting a putative multisensory zone (MZ) in parietotemporal cortex for integration of auditory and somatosensory responses.

The earlier work, based on extracellular mapping techniques, suggested the existence and location of MZ in the rat. However, it did not address the cellular physiology or neural circuitry underlying multisensory integration in this unique region. To this end, the present study used in vivo intracellular recording and retrograde tracing combined with extracellular mapping to clarify the functional anatomy of multisensory integration in the MZ at the cellular level. Our specific objectives were to (1) identify the location and limits of MZ producing the nonlinear ASEP by using high-resolution extracellular mapping, (2) assess the unimodal and/or multisensory response characteristics of cells within MZ by using in vivo intracellular recordings with sharp microelectrodes, (3) examine the relationship between intracellular postsynaptic potentials evoked by multisensory stimuli and the nonlinear ASEPs recorded at the cortical surface to understand their origin, and (4) label thalamocortical pathways underlying sensory convergence in the MZ by microinjections of wheat germ agglutinin conjugated to horseradish peroxidase (WGA-HRP). Portions of this work have appeared in abstract form (Brett-Green et al., 2000).

MATERIALS AND METHODS
Surgical preparation

Adult male Sprague-Dawley rats (250–350 g) were anesthetized to a surgical level with intramuscular injections of ketamine HCl (100 mg/kg) and xylazine (25 mg/kg), then placed into a stereotaxic frame with hollow ear bars. Supplemental injections were administered as required to maintain a surgical level of anesthesia. A unilateral craniotomy in the right hemisphere, extending from bregma to lambda and lateral to the temporal bone, widely exposed the parietotemporal cortex. The dura was reflected and the cortical surface bathed regularly with physiological saline. Body temperature was maintained with a regulated heating pad. Most animals were killed by anesthetic overdose at the conclusion of the experiment. Animals receiving tracer injections recovered from anesthesia and survived for 24–48 hours before being reanesthetized and perfused. All procedures followed University of Colorado Institutional Animal Care and Use Committee guidelines for the humane use of experimental subjects.

Stimulation

Auditory click stimuli were delivered with a high frequency piezoelectric speaker aligned with the contralat-

---

Abbreviations

AEP	auditory evoked potential		N1	first negative amplitude peak of sensory evoked potentials
AI	primary auditory cortex		OT	optic tract
AII	secondary auditory cortex		P1	first positive amplitude peak of sensory evoked potential
APt	anterior pretectum		PC	posterior commissure
ASEP	auditory/somatosensory evoked potential		Pf	parafascicular nucleus
ASEPmod	auditory/somatosensory evoked potential model		Po	posterior thalamic nucleus
CG	central gray		PoT	posterior nucleus, triangular part
CP	cerebral peduncle		SC	superior colliculus
EPSP	excitatory postsynaptic potential		SCP	superior cerebellar peduncle
Ha	habenula		SEP	somatosensory evoked potential
HiT	habenulointerpeduncular tract		Sg	suprageniculate nucleus
HypP	posterior hypothalamic area		SIbf	primary somatosensory cortex, barrel field
LGd, LGBd, LGNd	dorsal division of the lateral geniculate nucleus		SII	secondary somatosensory cortex
			SN	substantia nigra
LGv, LGBv	ventral division of the lateral geniculate nucleus		Vb	ventrobasal complex
LP	lateral posterior nucleus		Vpl	lateral division of the ventral posterior nucleus
MB	mamillary body		Vpm	medial division of the ventral posterior nucleus
MGd	dorsal division of the medial geniculate body		VpmPC	medial division of the ventral posterior nucleus (parvicellular part)
MGm	medial division of the medial geniculate body		WGA-HRP	wheat germ agglutinin-horseradish peroxidase
MGv	ventral division of the medial geniculate body		ZI	zona incerta
ML	medial lemniscus			
MZ	multisensory zone			

eral ear bar. Clicks were computer-controlled monophasic square-wave pulses (0.3 msec). Silent stimulation of the large vibrissae on the contralateral mystacial pad was achieved with a pulsed (0.5 msec) electromagnet. The large vibrissae were linked by a short ferrous wire approximately 25 mm from the mystacial pad. The wire was positioned 1.0 mm below the magnet, and stimulation displaced the vibrissae vertically by ~0.5 mm. Stimuli were delivered in approximate spatial register as the vibrissae were gathered toward the posterior side of the face near the ear bar where the speaker was positioned.

Field potential recording

Epipial maps of the AEP, SEP, and ASEP were recorded by using a flat multielectrode array consisting of 64 silver wires in an 8 × 8 grid (tip diameter, ~100 μm; interelectrode spacing, 500 μm) covering a 3.5 × 3.5 mm area. Recordings were referenced to a silver ball electrode secured over the contralateral frontal bone and were simultaneously amplified (×10,000), analog filtered (band-pass cut-off = −6 dB at 0.001 to 3,000 Hz, roll-off = 5 dB/octave) and digitized at 10 kHz. Evoked potentials were averaged over 50–100 randomized presentations of click, vibrissa, and click and vibrissa stimulation. Trials consisted of 25 msec of baseline and 175 msec of poststimulus activity. The click-evoked AEP and vibrissa-evoked SEP were used to align the array across animals consistently so that AI was beneath the caudolateral electrodes and SIbf was beneath the rostromedial electrodes. This placement permitted recording of evoked potentials from primary and secondary somatosensory and auditory cortex without repositioning.

Intracellular recording

Intracellular recordings were made in 21 animals by using a surface array with a central access hole to accommodate a microelectrode (see Fig. 5A). Microelectrodes were fabricated from thin-walled aluminosilicate glass pulled to 0.05 μm tip size (Sutter Instruments: P-87; Novato, CA). In 26 penetrations (n = 9 animals), electrodes were filled with 100 mM lidocaine, N-ethyl bromide quaternary salt (QX-314; Research Biochemicals; Natick, MA) in 2.0 M K$^+$-acetate. Iontophoresis used 100-msec depolarizing pulses of 2.0 nA at 2.0 Hz until all action potentials were blocked (Connors and Prince, 1982). This method permitted direct comparison of averaged intracellular postsynaptic potentials to the extracellular field potentials recorded at the surface without contamination of the average by action potentials. In 28 other penetrations (n = 12 animals), pipettes were filled with 1–2 M K$^+$-acetate-only to record action potentials and postsynaptic potentials. The in vivo impedances ranged from 80–120 MΩ. Recording and current injection was performed with an Axoclamp model 2-A amplifier (Axon Instruments; Foster City, CA) equipped with a 0.1 gain headstage (Axon Instruments: HS-2A). Microelectrodes were advanced perpendicularly into the cortex in 0.5-μm steps (100 mm/sec) by using a piezo translator compensated with a motor drive (WPI: Märzhäuser PM-10; Sarasota, FL) and a micrometer that indicated the approximate depth of the electrode tip. Criteria for an acceptable cell impalement were a resting membrane potential of at least −60 mV, overshooting action potentials with half amplitude widths less than 2.0 msec before QX-314 injection, and the ability to record for at least 30 minutes without hyperpolarizing

holding currents. Stimulation and recording parameters for combined intracellular and epipial recording were the same as those used for epipial recordings.

Histology

Small volumes (2.3–75 nl) of WGA-HRP (Sigma, 5.0%) were injected into the MZ through a glass micropipette (tip diameter, ~30 μm) by pressure using a Nanoliter 2000 microinjector (WPI; Sarasota, FL). Different points along the rostrolateral to caudomedial extent of the MZ were targeted in 15 animals. The tracer was delivered within cortical layers II/III–VI in 2.3-nl pulses. The animals survived for 24–48 hours after injection and were then perfused with 0.1 M phosphate buffer (50–100 ml, pH 7.4, room temperature,) followed by a 1.25% glutaraldehyde/1.0% paraformaldehyde buffered fixative solution (1,000 ml; 4–10° C).
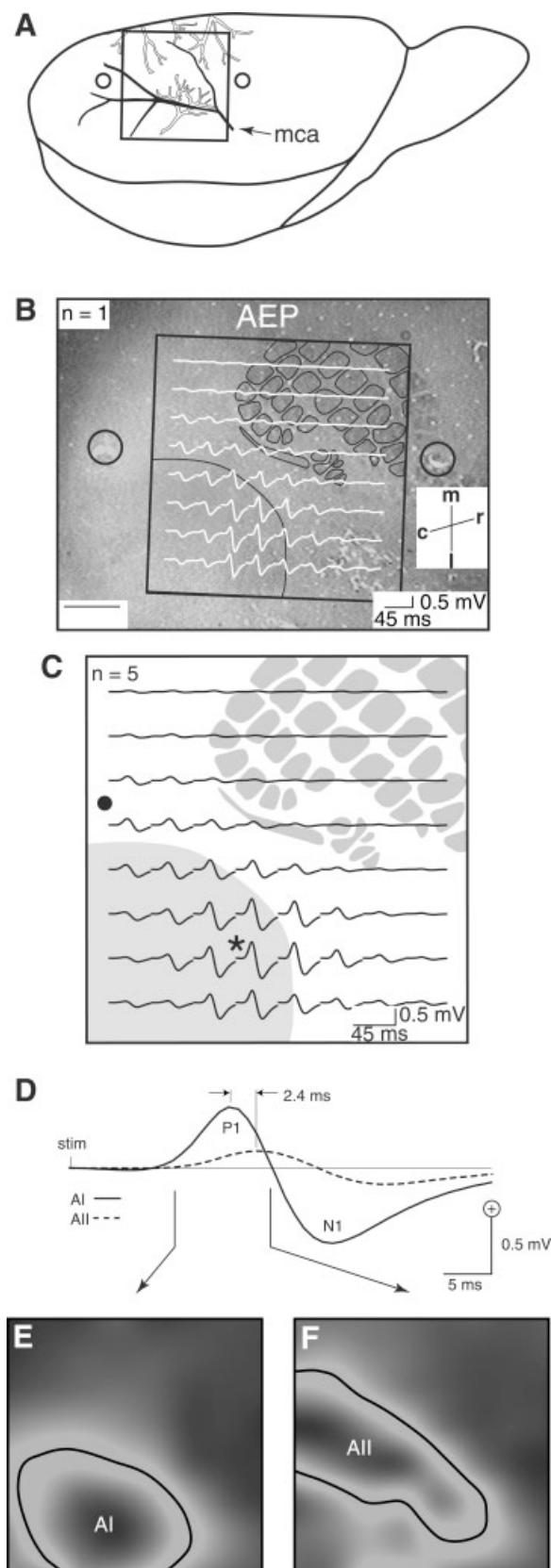
In five animals, the brains were removed from the skulls, blocked stereotaxically, sectioned coronally at 50 μm on a Vibratome, and processed with the tetramethylbenzidine (TMB) reaction for visualizing HRP (Mesulam, 1978). The sections were then mounted onto gelatinized slides, counterstained with neutral red, and cover-slipped. The labeled neurons were plotted on a Neurolucida computerized microscope with image analysis software (MicroBrightField, Inc., Colchester, VT), and representative sections were chosen for illustration (see Fig. 6).

In 11 animals, the brains were removed and the cortices were dissected and flattened between two glass slides. The cortex was cryoprotected in 30% sucrose in 0.1 M phosphate buffer (4–10°C). The right cortex was cut tangentially at 40 μm on a cryostat, and the sections were processed with a modified heavy metal diaminobenzidine/cytochrome oxidase recipe to identify WGA-HRP injection sites and to demarcate AI and SIbf (Adams, 1981; Wallace, 1987; Di and Barth, 1992). Sections were mounted onto gelatinized slides, dehydrated, and cover-slipped. Digital photos of layer IV were made for each of these experiments, and the location and extent of each injection site was plotted on a template (see Fig. 7). The remaining brainstem was blocked stereotaxically and sectioned coronally at 40 μm. Every other section was processed with TMB for visualizing HRP (Mesulam, 1978), mounted onto gelatinized slides, rapidly dehydrated, and cover-slipped. Intervening sections were stained with cresyl violet and cover-slipped. The retrogradely labeled thalamic cell bodies identified in individual sections were plotted under brightfield illumination, and their distribution was transferred onto a template of a corresponding coronal thalamic section (Swanson, 1992).

RESULTS

Extracellular recording

All recordings were made from the same location in parietotemporal cortex by using an alignment procedure based on vascular landmarks (Fig. 1A) and on the spatiotemporal distributions of both the AEP (Fig. 1B) and SEP (Fig. 2A). In Figure 1B, the AEP from one experiment was superimposed on a cytochrome oxidase–stained tangential section of cortical layer IV in the same animal. Fiducial marks made through tubes attached to the multielectrode array permitted the precise alignment of these data with the cortical recording site. A template of the cytochrome
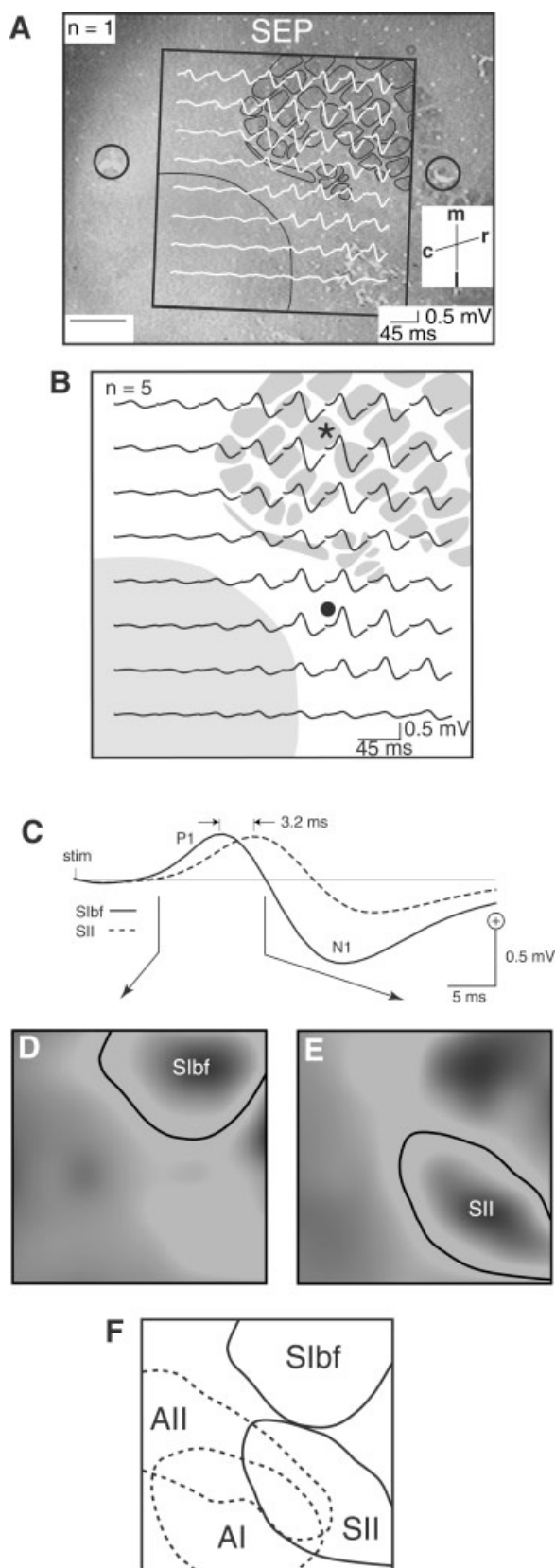
oxidase staining defining the anterodorsal border of AI and the barrels of SI was generated from this section for subsequent illustrative purposes.

Auditory stimulation alone elicited an AEP slow wave that was stereotyped in amplitude, morphology, and spatiotemporal distribution. The positive/negative amplitude peaks (P1 and N1, respectively) averaged across experiments (Fig. 1C) were largest in amplitude and shortest in poststimulus latency (Fig. 1D, solid trace) in electrodes over lateral AI (Fig. 1C, asterisk), as verified by cytochrome oxidase histology. This AEP distribution was consistent with previous studies: the largest amplitude/shortest latency responses lay in a cytochrome oxidase-positive patch of cortex receiving primary afferent projections from the MGv (Brett et al., 1994). Longer latency waveforms (Fig. 1D; dashed trace) at caudal electrode sites (Fig. 1C, black dot) were indicative of the activation of one or more secondary auditory fields. The average latency shift of the P1 in AII relative to AI was 2.4 ± 0.52 (SE) msec (n = 5; $P < 0.01$; t test). This latency shift was consistent with that found in previous studies where longer latency responses posterior and dorsal to AI were associated with cortex receiving parallel input from the dorsal division of the medial geniculate body (MGd; Brett et al., 1994). Here, a normalized isopotential map computed at 11.0-msec poststimulus, before AII responded, indicates that the short latency AI response covered approximately 2.5 mm^2 at the lateral border of the array (Fig. 1E). A similar map for 20.0-msec latency, when the AII AEP was of maximum amplitude and the AI AEP was at zero potential, shows an AII response that extended diagonally from the most caudal part of the array along the medial and rostral borders of AI (Fig. 1F). In these and subsequent figures, the borders of auditory fields were estimated from the 50% isopotential line of the normalized map (Fig. 1E,F, black line). However, the active cortical region always exceeded these boundaries by 0.5–1.0 mm and likely reflected activation of several auditory fields identified in the rat, including the anterior auditory and the posterior dorsal auditory areas (Horikawa et al., 1988). Because no tonotopic mapping was performed here, no distinction was made between the possible AI subfields or the secondary auditory fields.

The SEP slow wave had a positive/negative morphology (Fig. 2A) that resembled the AEP, except the averaged

Fig. 1. Surface topography and the auditory evoked potential (AEP). **A:** A lateral view of the right hemisphere, showing the middle cerebral artery (mca). **B:** The AEP superimposed on a cytochrome oxidase–stained tangential section of layer IV in the same animal. **C:** The AEP averaged across experiments and superimposed on a cytochrome oxidase template to define the approximate boundary of AI and SIbf. The average AEP had the largest amplitude and the shortest poststimulus latency in AI (asterisk), with lower amplitude and longer latency responses in AII (black dot). The characteristic delayed response of AII extended from the caudomedial to rostrolateral regions of the array and between AI and SIbf. **D:** The initial positive component (P1) of the average AEP in AII (dashed trace) was shifted by 2.4 msec relative to AI (solid trace). Arrows denote normalized isopotential plots in E and F. **E:** A normalized isopotential map of the AEP distribution at 11.0-msec poststimulus, with a short latency response in AI and no activity in AII. The black line represents 50% amplitude and is an estimate of the borders of AI. **F:** A similar map computed when the AEP was at maximum in AII and zero in AI. m, medial; r, rostral; l, lateral; c, caudal. For other abbreviations, see the list. Scale bar in B = 1 mm.

SEP (Fig. 2B) included two amplitude maxima. The earliest response (Fig. 2C, solid trace) was in central SIbf (Fig. 2B, asterisk) as verified by cytochrome oxidase histology. The other peak (Fig. 2C, dashed trace) was lateral to SIbf (Fig. 2B, black dot), near the classic location of SII (Welker and Sinha, 1972). The response extended into secondary somatosensory areas recently identified in the rat, possibly including the parietal lateral and the parietal medial regions (Koralek et al., 1990; Fabri and Burton, 1991a). The average P1 latency shift in the vibrissal SII relative to SIbf was 3.2 ± 0.35 (SE) msec (n = 5; $P < 0.01$; t test). Short- and long-latency isopotential maps showed that the SEP in SIbf (Fig. 2D) and SII (Fig. 2E) were ~ 2.0 mm apart in the medial and lateral rostral regions of the array, respectively. The locations and borders of AI and AII (Fig. 2F, dashed contours) and SIbf and the vibrissal SII (Fig. 2F, solid contours), defined by using isopotential plots, revealed that auditory and somatosensory evoked responses occurred in a common cortical zone near the center of the array.

When auditory and somatosensory stimuli were presented concurrently, the ASEP appeared in all electrodes (Fig. 3A,B). Its average spatiotemporal distribution approximated the sum of the AEP and SEP evoked by unimodal stimulation (Fig. 3C, ASEPmod). However, the actual ASEP in the region of overlapping AEP and SEP (Fig. 3D, dark solid trace) was always smaller (maximum difference at P1 peak = 0.1 ± 0.04 (SE) mV, n = 5; $P < 0.01$; t test) and had a shorter poststimulus latency (maximum difference at N1 peak = 1.5 ± 0.13 (SE) msec, n = 5; $P < 0.01$; t test) than the linear model (Fig. 3D, light solid trace). This yielded a difference waveform (DIFF; Fig. 3D, dashed trace) when the ASEPmod was subtracted from the ASEP.

Nonlinear multisensory responses, reflected in difference waveforms (Fig. 4A,B), were used to estimate the location and extent of MZ. The normalized isopotential map of the maximum difference waveform ran diagonally from the caudomedial to rostrolateral regions of the array (Fig. 4C) and was centered on the area where both auditory and somatosensory responses were independently recorded (Fig. 4D, gray contour). This area was chosen for subsequent intracellular recording and tracer injection.

Intracellular recording

Figure 5A shows the 63-electrode surface array with a central access hole through which sharp electrodes were lowered into the MZ for simultaneous extra- and intracellular recording. The array was positioned by using the AEP and SEP, as in previous figures. Based on the design of the array and on our alignment procedure, we estimate

Fig. 2. As in Figure 1, but showing somatosensory evoked potentials (SEP). The SEP from one experiment (**A**) and averaged across all experiments (**B**) was of maximum amplitude and shortest poststimulus latency in SIbf (asterisk in B), with a longer latency response in the vibrissal SII (black dot in B). **C:** The P1 amplitude peak in SII (dashed trace) was 3.2 msec later than in SIbf (dark trace). Normalized isopotential maps show the approximate borders of SIbf (**D**) and SII (**E**). **F:** Boundaries of AI and AII (dashed contours) and SIbf and SII (solid contours) estimated from the evoked potential maps reveal substantial AEP and SEP overlap near the center of the recording array. m, medial; r, rostral; l, lateral; c, caudal. For other abbreviations, see the list. Scale bars in A,F = 1 mm.

that intracellular recordings were near the center of the MZ, just caudomedial to the highest amplitude difference waves. Because tracer injection was made in only one of

these experiments, the exact locations of intracellular recordings in other experiments were not available.

Almost all MZ cells (54 of 58; 93%) responded with EPSPs and/or action potentials to both auditory and somatosensory stimulation and to combined auditory/somatosensory stimulation and, therefore, were classified as multisensory. All cells receiving QX-314 (n = 26) were multisensory, responding with slow (40.0-msec duration) EPSPs to auditory (Fig. 5B, dark trace), somatosensory (Fig. 5C, dark trace), and combined stimulation (Fig. 5D, solid dark trace) that were concurrent with the P1/N1 wave of the surface response (Fig. 5B–D, light traces). The mean intracellular multisensory EPSP (Fig. 5D, solid dark trace) exceeded that from either auditory (2.3 ± 0.7 [SE] mV; n = 26; $P < 0.01$, t test) or somatosensory (4.1 ± 0.5]SE] mV; n = 26; $P < 0.01$) stimuli alone. The amplitude maximum of the multisensory EPSP had a shorter poststimulus latency than the unimodal auditory (5.8 ± 1.0 [SE] msec; n = 26; $P < 0.01$, t test) or somatosensory (5.1 ± 0.8 [SE] msec; n = 26; $P < 0.01$, t test) responses. EPSPs evoked by combined stimulation were also shorter (2.3 ± 0.4 [SE] msec; n = 26; $P < 0.01$, t test) and smaller (4.4 ± 0.7 [SE] mV; n = 26; $P < 0.01$, t test) than the linear sum of EPSPs evoked separately (Fig. 5D, dashed dark trace). In 2 of 28 multisensory cells not receiving QX-314, individual trials of evoked action potentials were recorded for off-line computation of poststimulus time histograms (PSTH; Fig. 5B–D, gray bars). Action potentials often occurred at the rising crest of EPSPs evoked by auditory (Fig. 5B) and somatosensory (Fig. 5C) stimuli alone, and combined stimulation (Fig. 5D) elicited more action potentials than either stimulus alone. The maximum number of action potentials during combined stimulation did not differ from that predicted from the sum of the unimodal PSTHs (Fig. 5D; open bars, lines on histogram), although the latency of the maximum was earlier, much like the averaged EPSPs.

The simultaneous surface potential and intracellular experiments confirm and extend the results when only surface mapping was performed (Figs. 1–4). The P1 ASEP peak (Fig. 5D, light solid trace) was larger than that of the AEP (Fig. 5B, light trace; 0.9 ± 0.2 [SE] mV; n = 26; $P < 0.01$, t test) and the SEP (Fig. 5C, light trace; 0.5 ± 0.2 [SE] mV; n = 26; $P < 0.01$, $t\beta\beta$ test), whereas the N1 peak of the ASEP was earlier than the AEP (2.0 ± 0.3 [SE] msec; n = 26; $P < 0.01$, t test) and SEP (1.2 ± 0.3 [SE] msec; n = 26; $P < 0.01$, t test). Nonlinear responses had amplitude differences of the P1 (0.1 ± 0.03 [SE] mV, n =
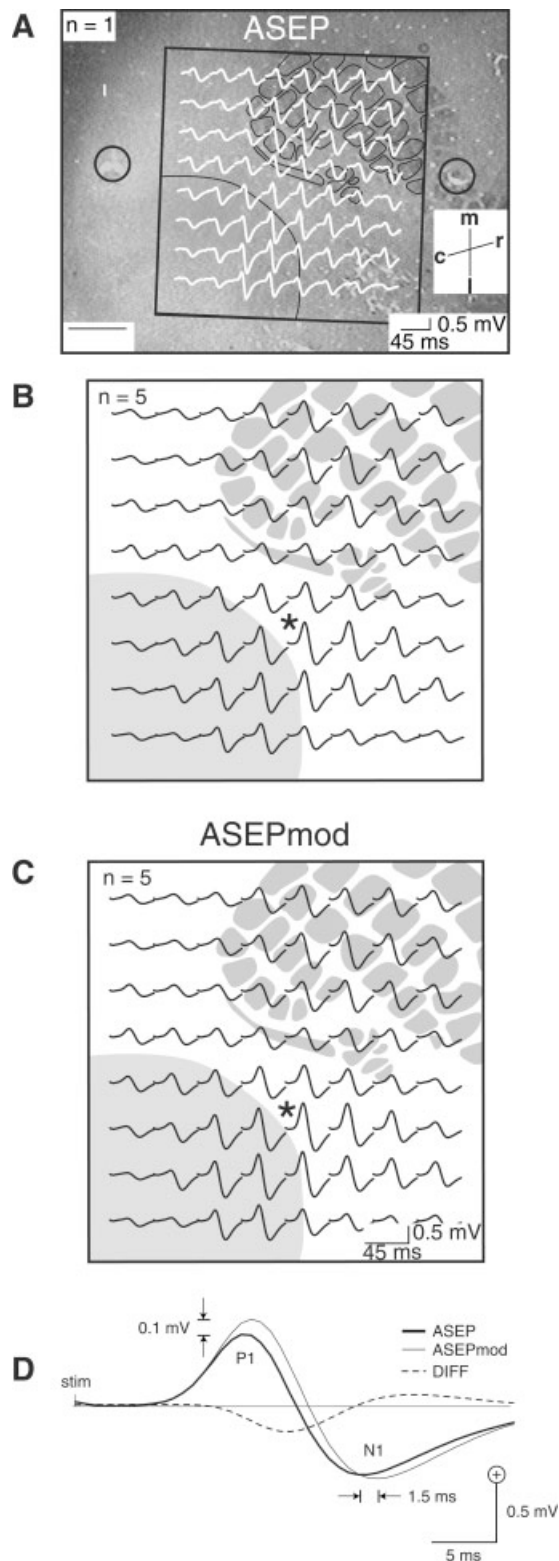

Fig. 3. Surface potentials evoked by concurrent auditory and somatosensory stimulation (ASEP) differ from their linear sum evoked by separate unimodal stimulation (ASEPmod). ASEPs from one experiment (**A**) and averaged across experiments (**B**) are widely distributed over the electrode array. **C:** The average ASEPmod calculated across experiments. The asterisk marks the channel chosen for ASEP and ASEPmod enlargements shown in D. **D:** The P1 component of the average ASEP (dark solid trace) between AI and SIbf (asterisk in B) has a lower amplitude than the ASEPmod (light solid trace) computed for the same electrode location (asterisk in C). The N1 component of the ASEP also has a shorter poststimulus latency than predicted by the linear model. Subtracting the ASEPmod from the ASEP yields a difference waveform (dashed trace), reflecting both the amplitude and latency differences. m, medial; r, rostral; l, lateral; c, caudal; DIFF, difference. For other abbreviations, see the list. Scale bar in A = 1 mm.
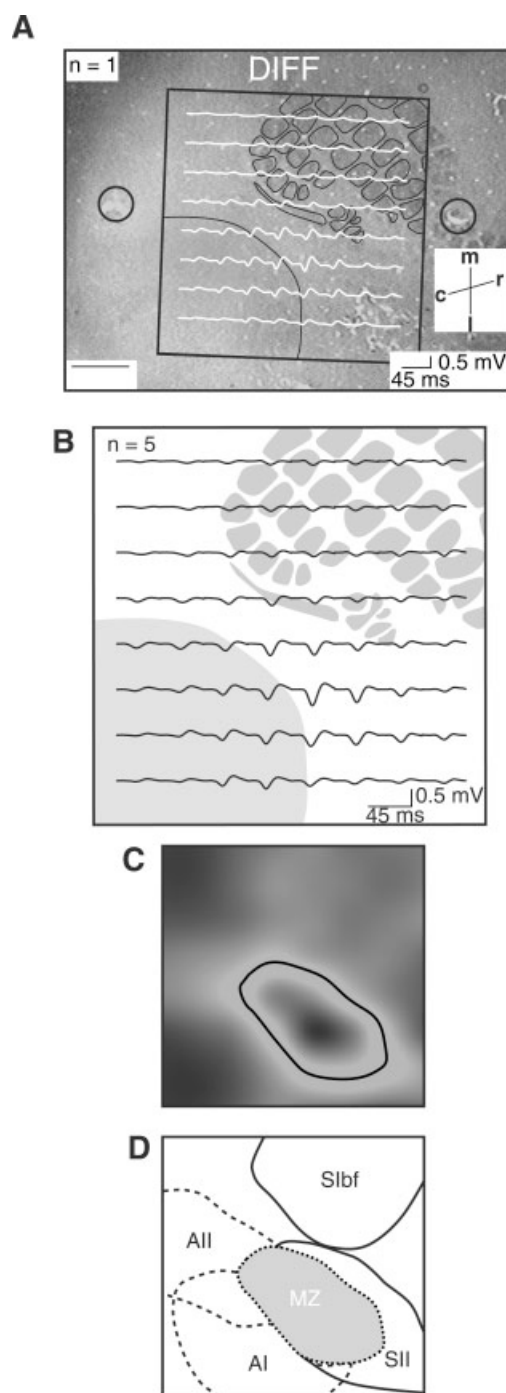
Fig. 4. The spatiotemporal distribution of difference (DIFF) waveforms is consistent across experiments and supports the hypothesis of a MZ. Difference waveforms were computed for one experiment (**A**) and averaged across experiments (**B**). **C:** An isopotential map of the maximum amplitude of the difference waveform was used to estimate the boundaries of MZ. **D:** MZ (light, dashed contour) is concentric with a zone of overlap between unisensory auditory (dark dashed contours) and somatosensory (solid contours) responses, near the center of the recording array. For abbreviations, see the list. Scale bar in A = 1 mm.

26; $P < 0.01$) and latency differences of the N1 (1.4 ± 0.2 [SE] msec, n = 26; $P < 0.01$) when the ASEP (Fig. 5D, light solid trace) was compared with the ASEPmod (Fig. 5D, light dashed trace). Concurrent difference waveforms for intracellular (Fig. 5E, solid dark trace) and extracellular (Fig. 5E, light solid trace) recordings were seen when the respective intra- and extracellular multisensory ASEPs were subtracted from the ASEPmods.

Connectional experiments

Coronal sections. To investigate thalamocortical projections to the MZ, WGA-HRP injections were made in 15 experiments (Table 1). Initially, we examined thalamocortical projections to the MZ in coronal sections. Cases 2, 3, 4, 5, and 7 showed retrograde labeling concentrated in the somatosensory thalamus, in the lateral segment of the ventral posterior lateral nucleus (Vpl), and in the dorsal segments of the ventral posterior medial nucleus (Vpm) and posterior nucleus (Po; Fig. 6C). Retrograde labeling was also present in the auditory thalamus, in the supra-geniculate nucleus (SG), and in the medial division of the medial geniculate nucleus (MGm; Fig. 6B,D). However, identification of the location and extent of individual injection sites within the MZ relative to the primary sensory areas was facilitated in tangential sections. In subsequent experiments, the cortex was sectioned tangentially and the remainder of the brain was sectioned coronally.

Cortical tangential and brainstem coronal sections. Tangential sections through layer IV processed with a modified diaminobenzidine/cytochrome oxidase recipe showed WGA-HRP injection sites relative to the borders of AI and SI. Electrophysiological recordings were aligned with these sections to verify the location of injections within MZ. A template depicting the location and diameter of each injection site was generated from individual digital photomicrographs of layer IV, confirming that most of the caudomedial to rostrolateral extent of the MZ was explored with WGA-HRP (Fig. 7). The retrograde labeling patterns for select thalamic coronal sections were plotted on corresponding atlas templates (Swanson, 1992; Fig. 8) to depict the results obtained for different injection sites within the MZ.

The injection site for case 17 (Fig. 8A) was near the caudomedial border of MZ. Retrograde labeling was concentrated in the somatosensory thalamus, in the lateral segment of the Vpl, and the dorsal segments of the Vpm and Po, in a pattern like that in the coronal cases. Analysis of the injection site indicated that it slightly overlapped rostral AI. Consequently, labeling was present in the acoustic thalamus, in the central portion of the MGv, and in the Sg and MGm. Similar retrograde labeling was obtained for other cases in the caudomedial MZ (Fig. 7, cases 13, 14), with more or less label present in the MGv, depending on the proximity of the injection to AI; case 15 was an exception. For two of these cases (Fig. 7, cases 14, 17), a small amount of label was also found in the MGd.
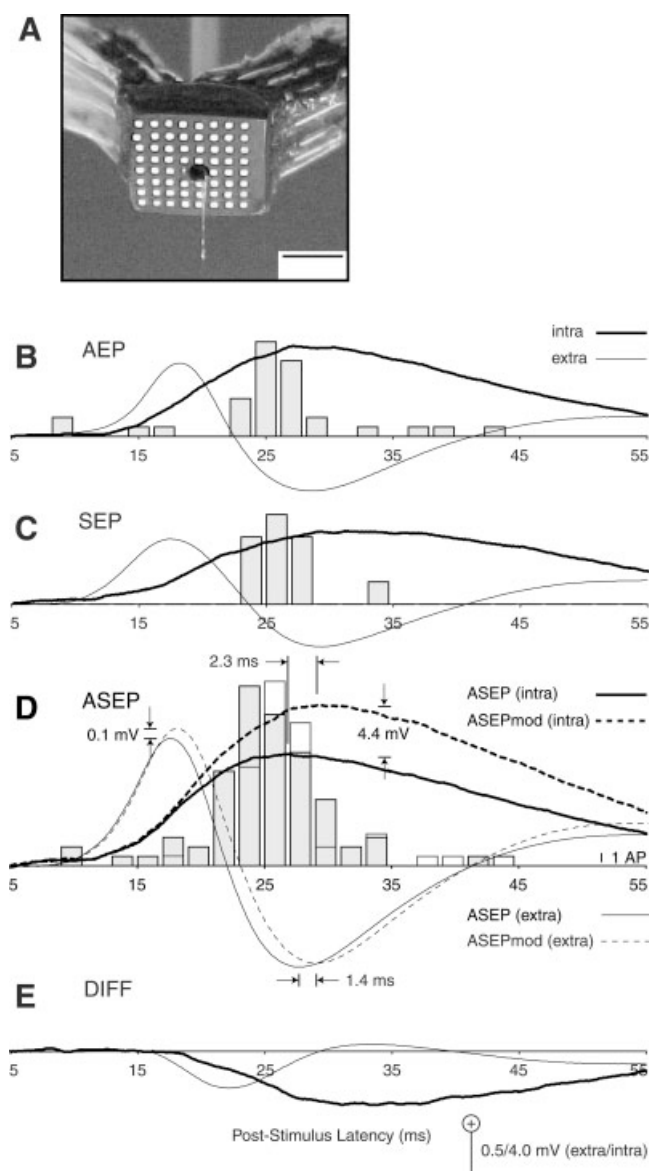
For case 16 (Fig. 8B), the injection site was centrally located within MZ. Retrograde labeling was found in the somatosensory thalamus but was more concentrated in the relevant segment of the Vpm, compared with that of the Vpl. A few cells were also present in the Po. As in case 17, labeling in the MGv was centrally located, but it was more extensive. Labeling was also present in the Sg and MGm of the acoustic thalamus. A small amount of label was apparent in the MGd. Similar retrograde labeling was

TABLE 1. Summary of Retrograde Labeling[1]

Case	WGA-HRP injection(nl)	Survival (hr)	Section (μm) cortex/ brainstem	DAB/ CO	Diameter injection site (mm)	Vpl	Vpm	Po	Sg	MGv	MGd	MGm
2[2]	50	30	50 c/c	−	−	+	+	+	+	−	−	+
3[2]	50	24	50 c/c	−	−	+	+	+	+	−	−	+
4[2]	30	24	50 c/c	−	−	+	+	+	X	X	X	X
5[2]	50	24	50 c/c	−	−	+	+	+	X	X	X	X
7[2]	75	42	50 c/c	−	−	+	+	+	+	−	−	+
13	11.5	48	40 tn/c	+	0.72	+	+	+	+	+	−	+
14	11.5	48	40 tn/c	+	0.83	+	+	+	+	+	+	+
15	11.5	24	40 tn/c	+	0.81	+	+	+	−	−	−	−
16	11.5	48	40 tn/c	+	0.68	−	+	+	+	+	+	+
17	11.5	48	40 tn/c	+	0.71	+	+	+	+	+	+	+
18	11.5	44	40 tn/c	+	0.65	+	+	−	+	+	−	+
19	9.2	24	40 tn/c	+	0.86	+	+	+	+	−	−	+
20	2.3	24	40 tn/c	+	0.62	+	+	+	+	+	−	+
25	4.6	24	40 tn/c	+	0.70	−	+	+	+	−	+	+
32	4.6	24	40 tn/c		0.65	+	+	−	+	−	−	+

[1]DAB/CO, diaminobenzidine/cytochrome oxidase. coronal section; tn, tangential section; X, record not available. For other abbreviations, see list.
[2]Injection sites not pictured relative to CO map of SI and AI.

Fig. 5. Intracellular recordings of multisensory responses in the MZ differ from the linear sum of potentials evoked by separate unimodal stimulation, much like surface recordings. **A:** A multielectrode array with a centralized access port for simultaneous recording of local intracellular and extracellular evoked responses in the MZ. **B:** A cell from the MZ after intracellular QX-314 injection produced slow excitatory postsynaptic potentials to auditory stimulation. The click-evoked EPSPs averaged across all cells (dark solid line) superimposed upon the grand average extracellular response recorded from a local surface electrode (light solid line). These data are superimposed on a poststimulus time histogram (PSTH) of action potentials evoked by auditory stimulation in an MZ cell that did not receive QX-314. **C:** MZ cells also produce slow EPSPs in response to somatosensory stimulation. The vibrissa-evoked EPSPs averaged across all cells (dark solid line) and the grand average extracellular response from a local surface electrode (light solid line). These responses are superimposed on the PSTH of action potentials evoked by somatosensory stimulation for the neuron in B. **D:** The average EPSPs evoked by concurrent auditory and somatosensory stimulation (dark solid line) exceeds the response evoked by either type of unimodal stimulation. In contrast to the linear model of the summed unimodal EPSPs (dark dashed trace), the multisensory EPSPs are smaller and peak earlier, as does the local extracellular multisensory response. As in the separately recorded results of Figure 3E, the average ASEP response (light solid line) is larger than either the AEP or SEP but is smaller and occurs earlier than the ASEPmod (light dashed line). The multisensory PSTH shows that more action potentials are elicited by combined stimulation and that they peak earlier. **E:** Subtraction of the intracellular ASEP from the linear model of the ASEP yields a difference waveform (dark line) as does subtraction of the extracellular ASEP from the linear model of the ASEP (light line). For abbreviations, see the list. Scale bar in A = 2 mm.

obtained for other cases with central injections in the MZ (Fig. 7, cases 18, 20), excepting labeling in the MGd.

The injection sites for cases 19 and 32 (Fig. 7) were at the rostrolateral border of MZ. As depicted for case 19 in Figure 8C, retrograde labeling was strongest in the somatosensory Vpl, Vpm, and Po, as well as in the Sg and MGm. Weak labeling was present in the MGv or the MGd. The labeling for an additional case (25) with an injection at the rostrolateral border of MZ can be seen in Figure 9A. It resembles the other two cases (19, 32), save for the absence of label in the Vpl and the presence of it in the MGd.

In summarizing the results of WGA-HRP injections in the MZ, the likely variability of individual sensory representations in the MZ must be noted. However, the Vpl,
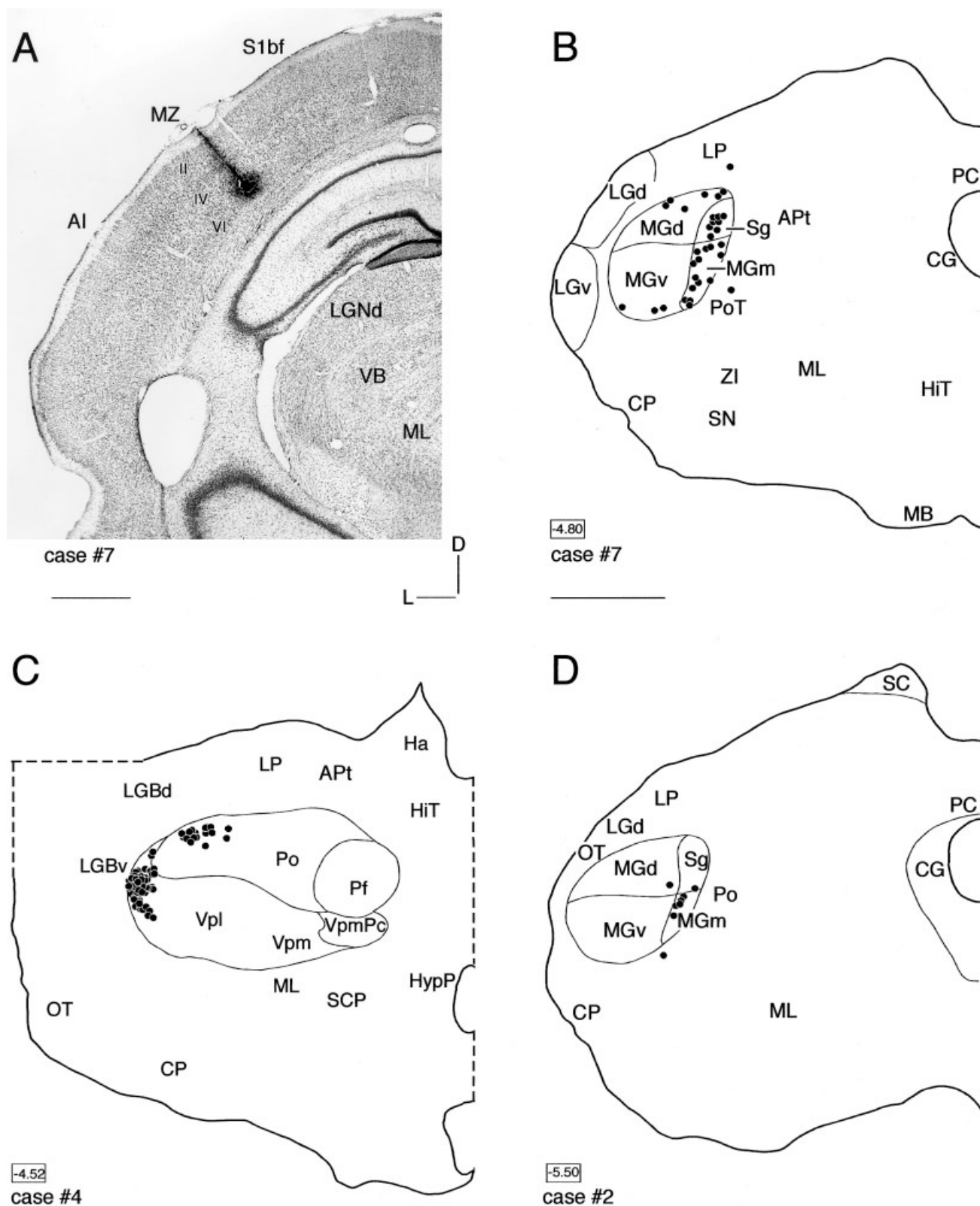
Fig. 6. Cytoarchitecture of MZ, a representative injection site, and characteristic patterns of retrograde thalamic labeling. **A:** MZ had a less developed layer V than AI and smaller cells than the barrel field. This deposit spanned all layers. Numbers in boxes indicate distances from bregma in millimeters. **B:** The labeling ensuing from the deposit shown in A. A heterogeneous group of cells was labeled in the MGd; the few scattered neurons at the base of MGv are just above the intralaminar thalamic nuclei. Each dot represents one labeled neuron. **C:** In a second case, the pattern for caudomedial MZ injections labeled cells concentrated at the margin of the Vpl and Vpm, with a smaller focus in nearby Po. **D:** Most labeled neurons were confined to MGm in this experiment. For abbreviations, see the list. Scale bar in A,B = 1 mm.
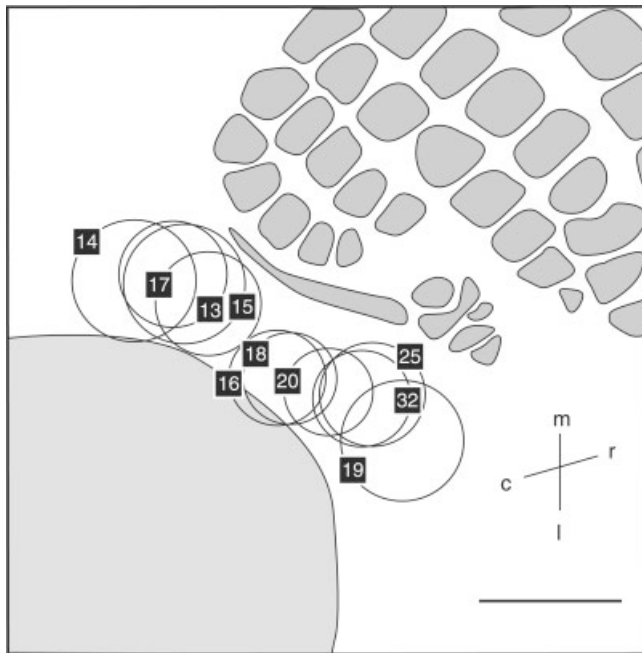
Fig. 7. Summary of WGA-HP injection sites in the MZ. Circles represent the approximate location and diameter of tracer injections for 10 experiments, as estimated from tangential cortical sections of layer IV processed with a modified diaminobenzidine/cytochrome oxidase protocol. m, medial; r, rostral; l, lateral; c, caudal. For other abbreviations, see list. Scale bar = 1 mm.

Vpm, Po, Sg, and MGm were consistently labeled for each of the MZ injections. The MGv was also labeled in most cases, whereas the MGd was rarely labeled. Although each injection in MZ labeled both somatosensory and acoustic nuclei, several trends were evident: Vpl labeling was strongest for caudomedial MZ injections, whereas Vpm labeling was strongest after rostrolateral MZ injections. Deposits near or impinging on AI labeled MGv, and a topographical organization of projections from the MGv was apparent. The most caudomedial MZ injections (cases 13, 14, 17) labeled the most lateral segment of the MGv, more central MZ injections (cases 16, 18) labeled the central MGv, and rostromedial MZ injections (case 20) labeled medial MGv. In contrast, the MGd was labeled mainly by caudomedial injections. Almost all MZ injections labeled primary as well as nonprimary thalamic nuclei, including the Po, Sg, and MGm. Sparse labeling was also present in some experiments in the ventromedial, ventrolateral, and central lateral thalamic nuclei. A striking anterograde pattern was evident in the superior colliculus, where exclusively anterograde labeling was noted in the deep layers (Fig. 9J). Otherwise, the distribution of anterograde labeling appeared largely reciprocal with the distribution of retrograde labeling in the somatosensory and auditory thalamus.

DISCUSSION
Extra- and intracellular multisensory responses in MZ

In surface maps, both the AEP and SEP have a positive/negative (P1/N1) slow wave characteristic of sensory evoked responses in most species (Allison and Hume, 1981). The P1/N1 components of the surface AEP and SEP have their largest peak-to-peak amplitude within AI and SIbf (Barth and Di, 1991; Di et al., 1994), where layer IV thalamocortical terminations are densest (Killackey, 1973; Patterson, 1977). These peaks likely represent the vertical flow of information in primary sensory cortex after the arrival of afferent input to layer IV (Rappelsberger et al., 1981; Mitzdorf, 1985; Vaknin, 1989; Barth and Di, 1990; Di et al., 1990). Both the AEP and SEP extend well beyond the primary sensory zones. Although there is currently disagreement on the precise location and borders of the several secondary auditory and somatosensory regions in the rat, the delayed evoked potentials recorded here indicate that secondary responses of both the AEP and SEP extend into the region between AI and SIbf.

AEP and SEP overlap alone does not necessarily indicate a multisensory zone, because it may simply reflect a mixed population of unisensory auditory and somatosensory cells. What does suggest a distinct multisensory responsiveness here is that the combined ASEP to stimulation does not equal the ASEPmod (the linear sum of the AEP and SEP). Prior work in rat cortex (Toldi et al., 1986; Di et al., 1994; Barth et al., 1995) found similar nonlinear multisensory responses. We also found a significant decrease in the poststimulus ASEP latency compared with the ASEPmod, with difference waveforms centered on the region overlap of AEP and SEP. These results are in accord with human event-related potential studies (Foxe et al., 2000) where a significant difference was found between responses to multisensory auditory/somatosensory stimulation and the summed unisensory auditory and somatosensory responses beginning at an early poststimulus latency. Together, these results suggest that high-resolution field potential mapping of nonlinear interactions is a sensitive method for identifying cortical sites for multisensory integration and is likely to be useful for the exploration of additional multisensory zones beyond the MZ described here.

The multisensory quality of MZ cells is verified by intracellular recording; nearly all cells in central MZ respond with EPSPs to both auditory and somatosensory, as well as combined stimulation. In addition, cells not given QX-314 respond to all stimulus conditions with EPSPs and action potentials. Intracellular EPSPs evoked in multisensory cells by combined stimulation have significantly larger amplitudes and shorter poststimulus latencies than those evoked by separate unisensory stimuli, much like the simultaneously recorded surface responses. This finding indicates that many MZ cells are multisensory, integrating EPSPs from the separate auditory and somatosensory pathways with an enhanced depolarization that can elicit suprathreshold responses at shorter poststimulus latencies than either modality alone. These data may indicate a mechanism for the behavioral observation in humans of faster responses to multisensory stimuli (Goldring et al., 1996; Giard and Peronnet, 1999).

The intracellular results also provide insight into the cellular basis of nonlinear ASEPs recorded at the cortical surface. The nonlinear interactions observed during the ASEP resemble those noted in previous reports (Toldi et al., 1984, 1986; Di et al., 1994; Jiang et al., 1994; Barth et al., 1995). Much like the saturation of multisensory responses in the superior colliculus (Perrault et al., 2000), the cortical response to multisensory stimulation is less
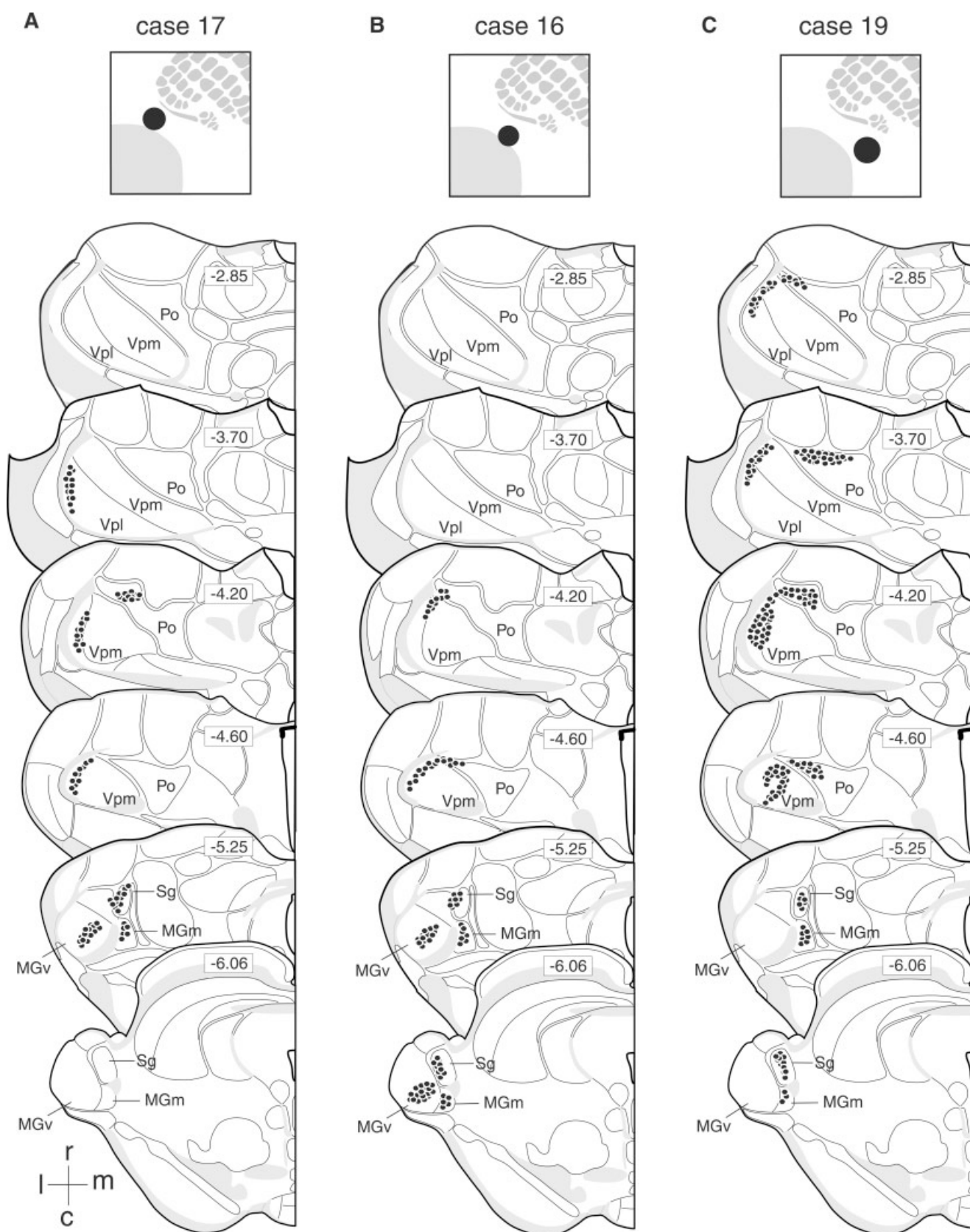
Fig. 8. Retrograde thalamic labeling patterns in representative cases. **A:** The neurons labeled after a caudomedial MZ injection (case 17) are shown on coronal templates from −2.85 to −6.06 mm caudal to bregma. Labeling is concentrated in the Vpl, Vpm, and Po of the somatosensory thalamus and in the MGv, Sg, and MGm, with a few cells in the MGd. Dots do not represent individual cells but the pattern of labeling. The numbers in boxes are distances from bregma.

B: The retrograde labeling for a central MZ injection (case 16). Labeling resembles A, except it is more concentrated in the Vpm compared with the Vpl, and there is more MGv labeling. **C:** The retrograde labeling from a rostrolateral MZ injection (case 19). Labeling is more extensive for this larger injection in the Vpl, Vpm, Po, Sg, and MGm, with none in MGv. m, medial; r, rostral; l, lateral; c, caudal. For other abbreviations, see the list.
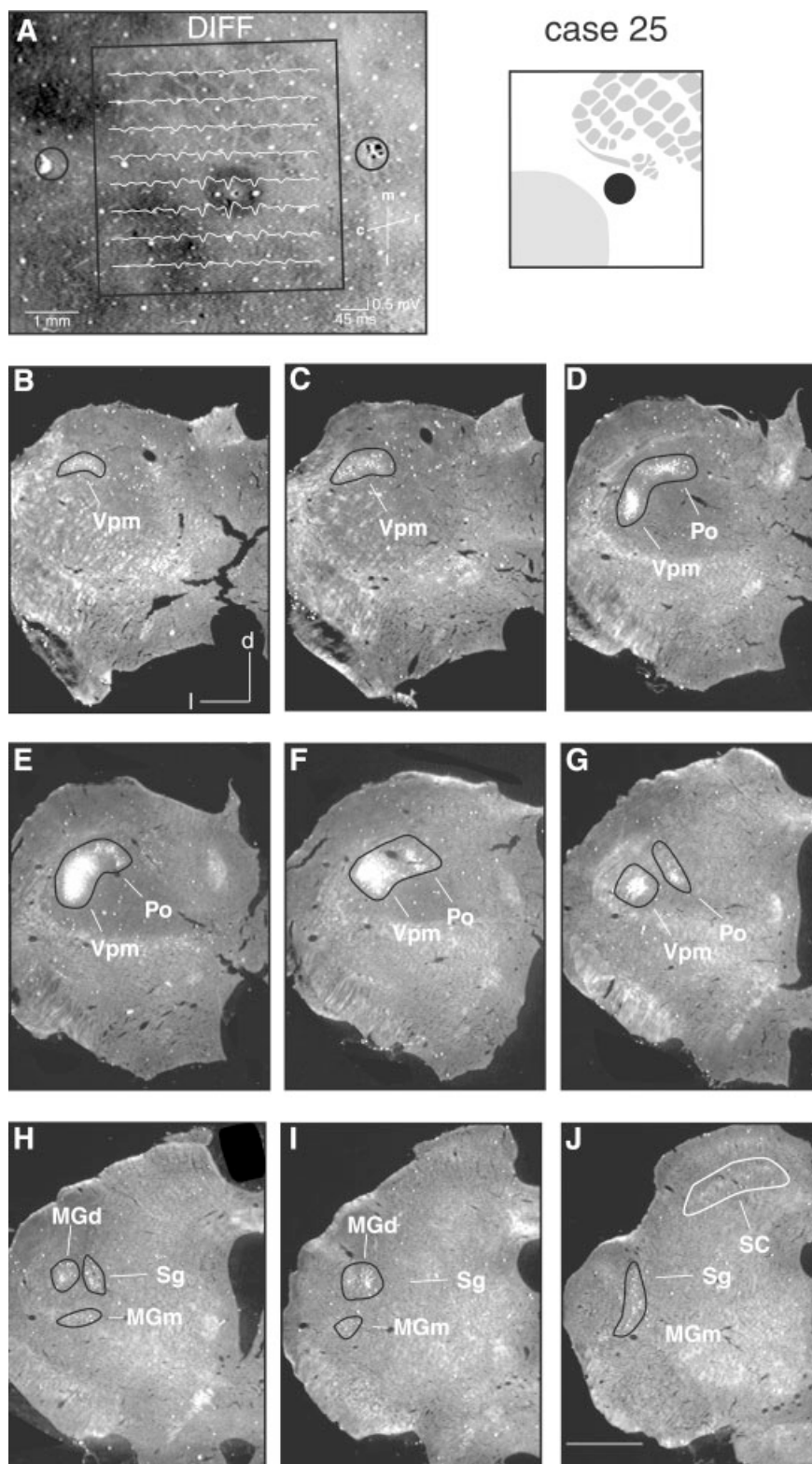
Fig. 9. WGA-HRP injection site in the MZ and retrograde labeling in the thalamus (case 25). **A:** Difference waves are aligned with an appropriate tangential cortical section of processed for WGA-HRP and cytochrome oxidase. The injection site is a dark oval centered approximately in the highest amplitude difference response region of the MZ. **B–J:** Darkfield photomicrographs of a rostral-to-caudal series of coronal sections show retrograde labeling in the main thalamic nuclei including Vpm, Po, MGd, Sg, and MGm (black outlines). Anterograde labeling in the SC appears in J (white outline). m, medial; r, rostral; l, lateral; c, caudal; DIFF, difference. For other abbreviations, see the list. Scale bar = 1 mm in J (applies to A–J).

than the sum of the unisensory responses. This intracellular nonlinearity probably reflects lower effective membrane resistance from many active synapses (Koch et al., 1983; Lev-Tov et al., 1983; Shepherd and Koch, 1990; Kogo and Ariel, 1999) combined with ionic driving forces of multisensory EPSPs that are less than the sum of unisensory EPSPs (Kuno and Miyahara, 1969; Lev-Tov et al., 1983), resulting in "sublinear" summation (Shepherd and Koch, 1990). The nonlinear ASEP may also reflect changes in the balance between excitatory and inhibitory influences on multisensory cells (Toldi et al., 1984) that are sensitive to the spatial register between auditory and somatosensory stimuli (Wallace et al., 1992; Stein and Wallace, 1996). However, whereas auditory and somatosensory stimuli were in approximate spatial register in the present experiment, systematic manipulation of their relative position, amplitude, or timing was not explored.

MZ and secondary sensory areas

Whether MZ is a distinct part of secondary somatosensory or auditory cortex cannot be resolved from these experiments. Our delineation of MZ based on surface evoked potentials overlaps several established subdivisions of SII (Koralek et al., 1990), and AII, as well as AI (Horikawa et al., 1988; Kelly, 1990). Although we defined the location and extent of the MZ based on click/vibrissae multisensory responsiveness, caudomedial MZ injections labeled cells in the Vpl trunk region. Some injection sites in MZ might have partially impinged on the spinal sector of SII. This possibility is consistent with observations that stimulation of the pinna, shoulder, and mid-trunk evokes responses near the caudomedial MZ (work in progress). Thus, the caudomedial border of MZ may relate to the parietal medial area (Barth et al., 1990; Koralek et al., 1990; Fabri and Burton, 1991a), a region between SI and primary visual cortex (VI) that has a topographic organization with the head represented laterally and the trunk medially. The MZ core defined here may correspond to a different subregion of SII, the parietal lateral region (Barth et al., 1990; Fabri and Burton, 1991a). Perhaps the parietal lateral region is an expanded vibrissal zone posterior to SI that overlaps the lateral edge of the parietal medial area. The rostrolateral MZ, on the other hand overlaps the posterior border of classically defined SII (Welker and Sinha, 1972). Thus, the relation of MZ to auditory fields identified in the rat is as yet incompletely defined. Several MZ injections labeled MGv. From these projections and the position of the MZ at the rostral border of AI, it is possible that part of MZ overlaps the anterior auditory field. However, a definitive distinction between AI and the anterior auditory field based on thalamocortical projection is not available in the rat. In addition, MZ injections labeled the MGd, MGm, and Sg, which have been shown by others (Niimi and Naito, 1974; Ryugo and Killackey, 1974; Raczkowski et al., 1975; Patterson, 1977; Winer and Morest, 1983; Winer and Larue, 1987; Arnault and Roger, 1990; Brett et al., 1994; Huang and Winer, 2000) to project to AII in the rat.

Our definition of MZ is also consistent with previous reports indicating that, in the rodent, classically defined SII has topographical overlap and multisensory response properties (Woolsey, 1967; Welker and Sinha, 1972; Carvell and Simons, 1986, 1987; Welker et al., 1988; Koralek et al., 1990). Surprisingly, these earlier electrophysiological studies found that body regions of SII were re-

sponsive to auditory stimulation, whereas the vibrissal (trigeminal) region of SII was largely unresponsive to auditory stimulation and received little or no input from the medial geniculate body. This discrepancy with our findings might reflect that the SII vibrissal region in the mouse is much smaller than the click/vibrissae MZ defined here and is separated from the auditory cortex (see Carvell and Simons, 1987; Fig. 1). An interesting, but unexplored, possibility is that the multisensory potential of cells in the MZ may include responsiveness to sensory stimulation of other body regions and/or other types of auditory stimulation. Further understanding of the MZ and its relationship to other sensory cortices will require more detailed analysis.

Sequential and parallel activation of MZ

Because evoked responses in secondary sensory cortex and in MZ are systematically delayed relative to primary cortex, there may a hierarchical sequence of activation dependent on ipsilateral intracortical feed-forward projections from primary to secondary and association regions. In fact, intracortical projections from AI to AII (Kolb, 1990; Mascagni et al., 1993; Romanski and LeDoux, 1993; Shi and Cassell, 1997) and from SIbf to SII (Akers and Killackey, 1978; Carvell and Simons, 1987; Chapin and Lin, 1990; Koralek et al., 1990; Fabri and Burton, 1991a; Kim and Ebner, 1999) probably contribute to their delayed evoked potentials. However, it is noteworthy that evoked responses in secondary sensory cortex and in MZ have the same positive/negative morphology as those in primary sensory cortex, characterizing thalamocortical activation of the middle cortical layers. The regions of AII abutting AI receive projections from the MGd and MGm as well as the Sg in the rat and cat (Niimi and Naito, 1974; Ryugo and Killackey, 1974; Raczkowski et al., 1975; Patterson, 1977; Winer and Morest, 1983; Winer and Larue, 1987; Arnault and Roger, 1990; Brett et al., 1994; Huang and Winer, 2000). There are also parallel thalamocortical projections to SII from the Vpm, Vpl, and Po (Tracey and Waite, 1995). In our experience, WGA-HRP injections near the classic SII labeled both the Vpm and Po. However, the labeled cells were clustered in the ventromedial part of these nuclei, whereas the MZ injections labeled mainly their dorsal segments (unpublished observations). Furthermore, electrical stimulation of the MGv and MGd selectively elicits localized responses in AI and posterior dorsal AII, respectively, and independent activation of either AI or AII does not evoke significant spread of such responses in anesthetized animals (Di and Barth, 1992). Also, there is physiological evidence for parallel activation of inputs to SII, as SI lesions do not abolish responses. These observations suggest that, whereas intracortical pathways must contribute to the delayed evoked responses in secondary cortex, these responses are also influenced by parallel thalamocortical projections. Because MZ is concentric with the region of overlap between SII and AII, the same reasoning suggests that parallel thalamocortical projections may contribute to its multisensory responsiveness.

Sensory convergence in the thalamus

Thalamic projections to MZ from the Vpm, Vpl, and MGv indicate that MZ receives unisensory information from the somatosensory and auditory relay nuclei. However, other input to MZ arise from Po, Sg, MGd, and MGm,

none of which is exclusively auditory. This finding suggests that some input to the MZ may reflect sensory convergence already present within the thalamus. Whereas the SIbf also receives input from both Po and Vpm (Fabri and Burton, 1991b), these fibers are from neurons in the ventromedial and medial part of Po and Vpm, respectively (Fabri and Burton, 1991b). As mentioned earlier, we found that only cells in the most dorsal parts of these nuclei project to MZ. These regions of the Po and Vpm, along with the Sg, MGd, and MGm, may constitute an integrative thalamic system independent of the unisensory somatosensory and auditory system (Winer and Morest, 1983). The strong input from multisensory thalamus to MZ in the rat indicates that the cortically recorded ASEP probably also reflects convergence occurring in multisensory thalamus. Nonlinear multisensory thalamic responses could contribute to ASEPs in the MZ much like those resulting from intracortical convergence.

Comparison of rat MZ with multisensory cortices of higher species

Some features of rat MZ recall properties of the cat anterior ectosylvian sulcus (Wallace et al., 1992) and possibly portions of the superior temporal plane in both monkeys and humans (Pandya and Yeterian, 1985; Krubitzer et al., 1995; Foxe et al., 2000; Schroeder et al., 2001), regions that also exhibit auditory and somatosensory convergence. Like the studies of cat multisensory cortex, our data further suggest that one downstream integrative role of the MZ may be to influence deep layers of the SC. It has been well established that visual, auditory, and somatosensory inputs reach the SC in a topographic manner so that each representation is in spatial register with the others. These sensory maps are intrinsically in register with motor maps, providing an efficient mechanism for cross-modal sensory integration and for mediating attentional and orienting behaviors. Perhaps this corticosubcortical network is analogous to the parietal cortex network for somatosensory integration in extrapersonal space. The MZ-SC system may provide a parallel pathway for egocentric auditory localization. Multisensory integration in the cat SC depends on projections from multisensory cortex (Wallace and Stein, 1994; Wilkinson et al., 1996; Jiang et al., 2001). If the rodent MZ is analogous to cat anterior ectosylvian sulcus, such projections could adaptively retune multisensory responses evoked by spatially coincident auditory and somatosensory stimuli, possibly directing auditory-guided movement.

ACKNOWLEDGMENTS

LITERATURE CITED

Adams JC. 1981. Heavy metal intensification of DAB-based HRP reaction product. J Histochem Cytochem 29:775.

Akers RM, Killackey HP. 1978. Organization of corticocortical connections in the parietal cortex of the rat. J Comp Neurol 181:513–538.

Allison T, Hume AL. 1981. A comparative analysis of short-latency somatosensory evoked potentials in man, monkey, cat, and rat. Exp Neurol 72:592–611.

Arnault P, Roger M. 1990. Ventral temporal cortex in the rat: connections of secondary auditory areas Te2 and Te3. J Comp Neurol 302:110–123.

Barth DS, Baumgartner C, Di S. 1990. Laminar interactions in rat motor cortex during cyclical excitability changes of the penicillin focus. Brain Res 508:105–117.

Barth DS, Di S. 1990. Three dimensional analysis of auditory evoked potentials in rat neocortex. J Neurophysiol 64:1527–1536.

Barth DS, Di S. 1991. The functional anatomy of auditory evoked potentials in rat neocortex. Brain Res 565:109–115.

Barth DS, Goldberg N, Brett B, Di S. 1995. The spatiotemporal organization of auditory, visual, and polysensory evoked potentials in rat cortex. Brain Res 678:177–180.

Benevento LA, Fallon J, Davis BJ, Rezak M. 1977. Auditory-visual interaction in single cells in the cortex of the superior temporal sulcus and the orbital frontal cortex of the macaque monkey. Exp Neurol 57:849–872.

Berman AL. 1961. Interaction of cortical responses to somatic and auditory stimuli in anterior ectosylvian gyrus of cat. J Neurophysiol 24:608–620.

Brett B, Di S, Watkins L, Barth DS. 1994. An HRP study of parallel thalamocortical projections responsible for the generation of midlatency auditory evoked potentials. Brain Res 647:65–75.

Brett-Green B, Walsh K, Barth DS. 2000. Polysensory cortex in the rat: field potential mapping and intracellular recording. Soc Neurosci Abstr 26:1976.

Bruce C, Desimone R, Gross CG. 1981. Visual properties of neurons in a polysensory area in superior temporal sulcus of the macaque. J Neurophysiol 46:369–384.

Carvell GE, Simons DJ. 1986. Somatotopic organization of the second somatosensory area (SII) in the cerebral cortex of the mouse. Somatosens Res 3:213–237.

Carvell GE, Simons DJ. 1987. Thalamic and corticocortical connections of the second somatic sensory area of the mouse. J Comp Neurol 265:409–427.

Chapin JK, Lin CS. 1990. The somatic sensory cortex of the rat. In: Kolb B, Tees RC, editors. The cerebral cortex of the rat. Cambridge: MIT Press. p 341–380.

Clemo HR, Stein BE. 1983. Organization of a fourth somatosensory area of cortex in cat. J Neurophysiol 50:910–925.

Connors BW, Prince DA. 1982. Effects of local anesthetic QX-314 on the membrane properties of hippocampal pyramidal neurons. J Pharmacol Exp Ther 220:476–481.

Di S, Barth DS. 1991. Topographic analysis of field potentials in rat vibrissa/barrel cortex. Brain Res 546:106–112.

Di S, Barth DS. 1992. The functional anatomy of middle latency auditory evoked potentials: thalamocortical connections. J Neurophysiol 68:425–431.

Di S, Baumgartner C, Barth DS. 1990. Laminar analysis of extracellular field potentials in rat vibrissa/barrel cortex. J Neurophysiol 63:832–840.

Di S, Brett B, Barth DS. 1994. Polysensory evoked potentials in rat parietotemporal cortex: auditory and somatosensory responses. Brain Res 64:267–280.

Fabri M, Burton H. 1991a. Ipsilateral cortical connections of primary somatic sensory cortex in rats. J Comp Neurol 311:405–424.

Fabri M, Burton H. 1991b. Topography of connections between primary somatosensory cortex and posterior complex in rat: a multiple flourescent tracer study. Brain Res 538:351–357.

Fishman MC, Micheal CR. 1973. Integration of auditory information in the cat's visual cortex. Vision Res 13:1415–1419.

Foxe J, Morocz I, Murray M, Higgins B, Javitt D, Schroeder C. 2000. Multisensory auditory-somatosensory interactions in early cortical processing revealed by high density electrical mapping. Cogn Brain Res 10:77–83.

Giard M, Peronnet F. 1999. Auditory-visual integration during multimodal object recognition in humans: a behavioral and electrophysiological study. J Cogn Neurosci 11:473–490.

Goldring J, Dorris M, Corneil B, Ballantyne P, Munoz D. 1996. Combined eye-head gaze shifts to visual and auditory targets in humans. Exp Brain Res 111:68–78.

Hikosaka K, Iwai E, Saito H-A, Tanaka K. 1988. Polysensory properties of neurons in the anterior bank of the caudal superior temporal sulcus of the macaque monkey. J Neurophysiol 60:1615–1637.

Horikawa J, Ito S, Hosokawa Y, Homma T, Murata K. 1988. Tonotopic representation in the rat auditory cortex. Proc Jpn Acad 64:260–263.

Huang C, Winer JA. 2000. Auditory thalamocortical projections in the cat: laminar and areal patterns of input. J Comp Neurol 427:302–331.

Hyvärinen J. 1982. Posterior parietal lobe of the primate brain. Physiol Rev 62:1060–1129.

Jiang H, Lepore F, Ptito M, Guillemot J. 1994. Sensory interactions in the anterior ectosylvian cortex of cats. Exp Brain Res 101:385–396.

Jiang W, Wallace MT, Jiang H, Vaughan JW, Stein BE. 2001. Two cortical areas mediate multisensory integration in superior colliculus neurons. J Neurophysiol 85:506–522.

Jones EG, Powell TPS. 1970. An anatomical study of converging sensory pathways within the cerebral cortex of the monkey. Brain 93:793–820.

Kelly JB. 1990. Rat auditory cortex. In: Kolb B, Tees RC, editors. The cerebral cortex of the rat. Cambridge: MIT Press. p 381–405.

Killackey HP. 1973. Anatomical evidence for cortical subdivisions based on vertically discrete thalamic projections from the ventral posterior nucleus to cortical barrels in the rat. Brain Res 51:326–331.

Kim U, Ebner FF. 1999. Barrels and septa: separate circuits in rat barrel field cortex. J Comp Neurol 408:489–505.

Koch C, Poggio T, Torre V. 1983. Nonlinear interactions in a dendritic tree: localization, timing, and role in information processing. Proc Natl Acad Sci U S A 80:2799–2802.

Kogo N, Ariel M. 1999. Response attenuation during coincident afferent excitatory inputs. J Neurophysiol 81:2945–2955.

Kolb B. 1990. Organization of the neocortex of the rat. In: Kolb B, Tees RC, editors. The cerebral cortex of the rat. Cambridge: MIT Press. p 21–34.

Koralek KA, Olavarria J, Killackey HP. 1990. Areal and laminar organization of corticocortical projections in the rat somatosensory cortex. J Comp Neurol 299:133–150.

Krubitzer L, Clarey J, Tweedale R, Elston G, Calford M. 1995. A redefinition of somatosensory areas in the lateral sulcus of macaque monkeys. J Neurosci 15:3821–3839.

Kuno M, Miyahara J. 1969. Non-linear summation of unit synaptic potentials in spinal motoneurones of the cat. J Physiol (Lond) 201:465–477.

Lev-Tov A, Miller J, Burke R, Rall W. 1983. Factors that control amplitude of EPSPs in dendritic neurons. J Neurophysiol 50:399–412.

Mascagni F, McDonald A, Coleman J. 1993. Corticoamygdaloid and corticocortical projections of the rat temporal cortex: a Phaseolus vulgaris leucoagglutinin study. Neuroscience 57:697–715.

Mesulam MM. 1978. Tetramethyl benzidine for horseradish peroxidase neurohistochemistry. A non carcinogenic blue reaction with superior sensitivity for visualizing neural afferents and efferents. J Histochem Cytochem 26:106–117.

Mesulam M-M. 1998. From sensation to cognition. Brain 121:1013–1052.

Mitzdorf U. 1985. Current source-density method and application in cat cerebral cortex: investigation of evoked potentials and EEG phenomena. Physiol Rev 65:37–100.

Niimi K, Naito F. 1974. Cortical projections of the medial geniculate body of the cat. Exp Brain Res 19:326–342.

Pandya DN, Yeterian EH. 1985. Architecture and connections of cortical association areas. In: Peters A, Jones EG, editors. Association and auditory cortices. New York: Plenum Press. p 3–61.

Patterson H. 1977. An anterograde degeneration and retrograde axonal transport study of the cortical projections of the rat medial geniculate body. Ph.D. Thesis: Boston, MA: Boston University.

Perrault TJ, Vaughan JW, Stein BE, Wallace MT. 2000. Dynamic response ranges in multisensory superior colliculus neurons. Soc Neurosci Abstr 26:1838.

Raczkowski D, Diamond IT, Winer J. 1975. Organization of the thalamocortical auditory system in the cat studied with horseradish peroxidase. Brain Res 101:345–354.

Rappelsberger P, Pockberger H, Petsche H. 1981. Current source density analysis: methods and application to simultaneously recorded field potentials of the rabbit's visual cortex. Pflugers Arch 389:159–170.

Roda JM, Reinoso-Suárez F. 1983. Topographical organization of the thalamic projections to the cortex of the anterior ectosylvian sulcus in the cat. Exp Brain Res 49:131–139.

Romanski L, LeDoux J. 1993. Information cascade from primary auditory cortex to the amygdala: corticocortical and corticoamygdaloid projections of temporal cortex in the rat. Cereb Cortex 3:515–532.

Ryugo DK, Killackey HP. 1974. Differential telencephalic projections of the medial and ventral divisions of the medial geniculate body of the rat. Brain Res 82:173–177.

Schneider AS, Davis JL. 1974. Interactions of the evoked responses to visual, somatic and auditory stimuli in polysensory areas of the cat cortex. Physiol Behav 13:365–372.

Schroeder CE, Lindsley RW, Specht C, Marcovici A, Smiley JF, Javitt DC. 2001. Somatosensory input to auditory association cortex in the macaque monkey. J Neurophysiol 85:1322–1327.

Shepherd GM, Koch C. 1990. Dendritic electrotonus and synaptic integration. In: Shepherd GM, editor. The synaptic organization of the brain. Oxford: Oxford University Press. p 439–473.

Shi C, Cassell M. 1997. Cortical, thalamic, and amygdaloid projections of rat temporal cortex. J Comp Neurol 382:153–175.

Stein BE, Meredith MA. 1993. The merging of the senses. Cambridge: MIT Press.

Stein B, Wallace M. 1996. Comparisons of cross-modality integration in midbrain and cortex. Prog Brain Res 112:289–299.

Steriade M, Jones EG, McCormick DA. 1997. Thalamus. Amsterdam: Elsevier.

Swanson LW. 1992. Brain maps: structure of the rat brain. Amsterdam: Elsevier.

Toldi J, Fehér O. 1984. Acoustic sensitivity and bimodal properties of cells in the anterior suprasylvian gyrus of the cat. Exp Brain Res 55:180–183.

Toldi J, Fehér O, Feuer L. 1984. Dynamic interactions of evoked potentials in a polysensory cortex of the cat. Neuroscience 13:645–652.

Toldi J, Fehér O, Wolfe JR. 1986. Sensory interactive zones in the rat cerebral cortex. Neuroscience 18:461–465.

Tracey DJ, Waite PME. 1995. Somatosensory system. In: Paxinos G, editor. The rat nervous system. San Diego: Academic Press. p 689–704.

Vaknin G. 1989. Major excitatory pathways in rat visual cortex. Ph. D. Thesis: Kent, OH: Kent State University.

Wallace MN. 1987. Histochemical demonstration of sensory maps in the rat and mouse cerebral cortex. Brain Res 418:178–182.

Wallace MT, Stein BE. 1994. Cross-modal synthesis in the midbrain depends on input from the cortex. J Neurophysiol 71:429–432.

Wallace MT, Meredith MA, Stein BE. 1992. Integration of multiple sensory modalities in cat cortex. Exp Brain Res 91:484–488.

Welker C, Sinha MM. 1972. Somatotopic organization of SmII cerebral neocortex in albino rat. Brain Res 37:132–136.

Welker E, Hoogland PV, Van der Loos H. 1988. Organization of feedback and feedforward projections of the barrel cortex: a PHA-L study in the mouse. Exp Brain Res 73:411–435.

Wilkinson LK, Meredith MA, Stein BE. 1996. The role of the anterior ectosylvian sulcus in cross-modality orientation and approach behavior. Exp Brain Res 112:1–10.

Winer JA, Larue DT. 1987. Patterns of reciprocity in auditory thalamocortical and corticothalamic connection: study with horseradish peroxidase and autoradiographic methods in the rat medial geniculate body. J Comp Neurol 257:282–315.

Winer JA, Morest DK. 1983. The medial division of the medial geniculate body of the cat: implications for thalamic organization. J Neurosci 3:2629–2651.

Woolsey TA. 1967. Somatosensory, auditory and visual cortical areas of the mouse. Johns Hopkins Med J 121:91–112.